Ventricular activity cancellation in electrograms during atrial fibrillation with constraints on residuals' power

Valentina D.A. Corino [a,*], Massimo W. Rivolta [b], Roberto Sassi [b],
Federico Lombardi [c], Luca T. Mainardi [a]

[a] *Dipartimento di Elettronica, Informazione e Bioingegneria, Politecnico di Milano, 20133 Milan, Italy*
[b] *Dipartimento di Informatica, Università degli Studi di Milano, 26013 Crema, Italy*
[c] *Cardiologia, Dipartimento di Scienze della Salute, Università degli Studi di Milano, 20142 Milan, Italy*

ARTICLE INFO

ABSTRACT

During atrial fibrillation (AF), cancellation of ventricular activity from atrial electrograms (AEG) is commonly performed by template matching and subtraction (TMS): a running template, built in correspondence of QRSs, is subtracted from the AEG to uncover atrial activity (AA). However, TMS can produce poor cancellation, leaving high-power residues. In this study, we propose to modulate the templates before subtraction, in order to make the residuals as similar as possible to the nearby atrial activity, avoiding high-power ones. The coefficients used to modulate the template are estimated by maximizing, via Multi-swarm Particle Swarm Optimization, a fitness function. The modulated TMS method (mTMS) was tested on synthetic and real AEGs. Cancellation performances were assessed using: normalized mean squared error (NMSE, computed on simulated data only), reduction of ventricular activity (VDR), and percentage of segments (PP) whose power was outside the standard range of the atrial power. All testings suggested that mTMS is an improvement over TMS alone, being, on simulated data, NMSE and PP significantly decreased while VDR significantly increased. Similar results were obtained on real electrograms (median values of CS1 recordings PP: 2.44 vs. 0.38 $p < 0.001$; VDR: 6.71 vs. 8.15 $p < 0.001$).

1. Introduction

Atrial fibrillation (AF), the most common arrhythmia encountered in the clinical practice, is characterized by a highly irregular atrial activity. Despite the apparently random activation pattern, numerous studies revealed the presence of an underlying order induced by factors such as myocardium anatomy, electrophysiological properties, and autonomic innervation. It has been suggested that the level of irregularity depends on the number of circulating wavefronts in the atria and its quantification can be used to classify AF events (from type-I to type-III according to Wells' classes [1]). In addition, indices of organization may be related to the electrophysiological mechanisms sustaining AF, thus they could be used to predict spontaneous termination of AF or the response to ablation therapy [2].

To assess the level of atrial activity (AA) organization, several signal processing methods were developed in the last years [3]. AF organization can be described in terms of various characteristics of electrical activity of the fibrillating atria, such as the repeatability/regularity of the atrial activations [4–6], the correlation/synchronicity among electrograms recorded in different locations [7–9], or the similarity of the wave morphology [10].

In most cases the first pre-processing step in these techniques is the cancellation of the ventricular activity (VA) superimposed to the atrial one. Most studies [3,11,12] commonly performed this operation by means of template matching and subtraction (TMS). Briefly, a running template is obtained by adaptive averaging AEG segments, taken in correspondence of QRS complexes on a concurrent surface ECG recording [13]. Finally, the template is subtracted from the endocardial recordings. TMS is both simple and effective. In fact, it is sufficiently resistant to baseline fluctuations outside the QRS complex or R-peak time misalignments. However, there are situations in which a good cancellation is not achieved by TMS and the residuals may corrupt the successive analysis. An example of this is when the morphology of successive ventricular beats on the AEG is very variable in duration and/or amplitude.

Other methods have been proposed for VA cancellation. An adaptive finite-impulse response filtering can be used: the filter operates on the reference channel (lead II of the surface ECG) to produce an estimate of the interference, which is then subtracted from the AEG. However, this method strongly depends on having an adequate additional reference signal for cancellation. Moreover, baseline fluctuations outside the QRS complex or R-peak time misalignments lead to a decrease in performance [13]. An approach

* Corresponding author. Tel.: +39 02 23993392; fax: +39 02 23993360.
  E-mail address: valentina.corino@polimi.it (V.D.A. Corino).

based on independent component analysis was also suggested by [13], as long as during AF atrial and ventricular activities can be considered as decoupled electrical processes that appear mixed at the electrode output. Unfortunately, all these methods can fail in a few cases (for example for R-peak time misalignments), independently of the AF type or ventricular rate, thus leaving ahead residues with localized high power and spoiling the following analysis [13,8]. The problem is similarly encountered when extracting the atrial activity in surface ECGs [14,15].

We have recently observed better performances when the templates were modulated by a set of coefficients [16]. Aim of this work is to improve the quality of the VA subtraction performed by TMS by reducing the occurrence of localized spurious residuals. To do so, the TMS template is modulated by a set of coefficients, so that the residue is as similar as possible to the nearby atrial activity, avoiding high-power residuals. Coefficients were estimated maximizing a fitness function, via Multi-swarm Particle Swarm Optimization (MPSO) [17].

2. Methods

2.1. VA cancellation

In the following, AEGs recorded during AF are modeled as

$$s(n) = a(n) + v(n) = a_L(n) + a_B(n) + v(n) \qquad (1)$$

where $a(n)$ is the sum of a_L, the localized AA, and a_B the background, wide-band AA, and $v(n)$ is the VA. The localized AA represents an atrial depolarization occurring close to the electrodes, and the mean inter-a_L interval is the inverse of the AF frequency. On the other hand, the background AA represents the far-field effects on the electrodes, plus noise.

During AF, $a(n)$ and $v(n)$ overlap in time and thus cancellation of $v(n)$ is required to uncover the atrial components. In the traditional and widely used TMS method, a template $t(n)$ is built by adaptive averaging of AEG segments taken in correspondence of QRSs on surface ECG. The template can be built using a fixed number of preceding ventricular complexes. However we chose here an equivalent method based on a recursive numeric filter:

$$t(n) = t(n-1) + \gamma[s(n) - t(n-1)], \qquad (2)$$

where the two signals $s(n)$ and $t(n-1)$ are previously aligned through cross-correlation. The parameter γ weights the innovation at time n with respect to the template at the time $n-1$. Setting $\gamma = 0.1$, as employed, is substantially equivalent to taking the average of 20 nearby QRSs complexes, a number found sufficient to reduce the effects of uncorrelated noise [11,15]. Coherently, the first template $t(0)$ is obtained as the average, after alignment, of the first twenty QRSs. It is worth noting that before subtraction, baseline wander has to be removed from the original signal.

The running template is subtracted from the AEG $s(n)$. The resulting quantity

$$r(n) = s(n) - t(n) = a(n) + [v(n) - t(n)] \qquad (3)$$

is called *residue* and will contain atrial contributions only when $t(n) \approx v(n)$, i.e., when the template is a good estimator of the VA.

2.2. Modulation of the template

In our approach, instead of subtracting $t(n)$, we used a modulated version. If $\mathbf{t} = [t(1), \ldots, t(N)]^T$ is the template, N being the number of samples, our estimator of the VA becomes
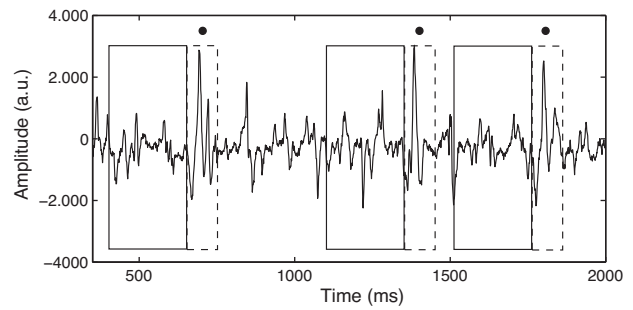
$$\mathbf{v} = \mathbf{Wt}, \qquad (4)$$

Fig. 1. AEG signal recorded during an ablation procedure (CS1). Different portions of the AEG are highlighted: (i) 250 ms of atrial signal without VA (portion of the signal in the solid rectangle), (ii) 100 ms of residual signal centered in the VA (portion of the signal in the dashed rectangle). A clear influence of VA can be noted in correspondence to QRS complexes (black dots).

where the diagonal $N \times N$ matrix $\mathbf{W}$ is the weighting matrix, whose elements need to be estimated at each beat. $\mathbf{W}$ modulates $\mathbf{t}$ and thus it can help in keeping the residual power in the standard range of AA power, reducing it when the actual VA on AEG differs markedly from the template. To estimate $\mathbf{W}$, the residual signal is compared to a portion of signal not containing VA; thus two segments of AEG are considered: (i) 250 ms of atrial signal without VA (portion of signal inside the rectangle with solid line in Fig. 1), (ii) 100 ms of residual signal centered in the VA (portion of signal inside the rectangle with dashed line in Fig. 1). Clearly, $\mathbf{W} \equiv \mathbf{I}$ in the classic TMS. The weighting matrix $\mathbf{W}$ is obtained by maximizing, via Multi-swarm Particle Swarm Optimization (see Appendix), a fitness function J. The objective of cancellation is to obtain a residual signal, which is as similar as possible to the nearby atrial activity, avoiding high-power residuals. We also desire the final template to be not too different from the one provided by TMS, to improve robustness to outliers (which are less likely to corrupt the mean pattern). Given the complexity of the task, a multiobjective optimization approach was adopted and a proper fitness function J was designed. This fitness function was therefore composed of three terms, each reflecting one of the objectives just stated: (i) constraining the power of the residues (J_1) and (ii) of their first derivative (J_2), and (iii) limiting the deformation on the TMS template (J_3). In detail, J is defined as the sum of three factors:

$$J(\mathbf{W}) = \alpha J_1(\mathbf{W}) + \beta J_2(\mathbf{W}) + \delta J_3(\mathbf{W}). \qquad (5)$$

Let us first define the function $j(\cdot)$ as

$$j(\rho) = \begin{cases} 1, & \rho \leq 1 \\ -(\rho - 1)^3, & \rho > 1. \end{cases} \qquad (6)$$

The function $j(\rho)$ becomes closer to the value of 1 as long as ρ decreases towards 1. Please note, that the derivative of j is not constant. (This will prove useful in the following as the convergence velocity in the optimization procedure will be higher when $\rho \gg 1$, and will decrease when ρ gets closer to 1.)

Then we defined the mean power of the discrete signal $\mathbf{x} = [x(1), \ldots, x(N)]$ as

$$P_x = \frac{1}{N} \sum_{k=1}^{N} x(k)^2 \qquad (7)$$

where N is the number of samples.

The first term in the fitness function of Eq. (5)

$$J_1 = j(\rho_1), \quad \rho_1 = \frac{P_r}{P_a} \qquad (8)$$

quantifies the similarity between the power of the residual signal and the power of the AEG where only AA is present. P_r and P_a

are the mean power of the residue and the atrial signal, respectively. The AEG segment where only AA is present is defined as the one in the temporal window preceding the VA to be canceled ($[-300\,\text{ms}\ -50\,\text{ms}]$, considering as 0 the position of the peak of VA) as shown in Fig. 1.

The second term J_2 quantifies the discrepancy in the derivatives of the residue and that of the AEG when no VA is present. Similar to Eq. (8), it is defined as

$$J_2 = j(\rho_2), \quad \rho_2 = \frac{P_{D_r}}{P_{D_a}}, \tag{9}$$

where D_r and D_a are the derivatives of the residue and the atrial signal, respectively, and P_{D_r} and P_{D_a} their powers. The first derivative of a discrete signal $\mathbf{x}$ was approximated by

$$D_x(k) = x(k+1) - x(k) \tag{10}$$

where $k = [1, \ldots, N-1]$.

Finally, J_3 is used to constrain v to remain close to the original template $\mathbf{t}$:

$$J_3 = j(\rho_3) - 1, \quad \rho_3 = \frac{d(\mathbf{t}, v)}{\theta}. \tag{11}$$

The metric

$$d(x, y) = \frac{1}{\pi} \arccos\left(\frac{\mathbf{x}^T \mathbf{y}}{\|\mathbf{x}\|\|\mathbf{y}\|}\right) \tag{12}$$

measures the distance between the two discrete signals $\mathbf{x}$ and $\mathbf{y}$. An alternative metric could have been the mean square error of the difference signal, but we rather preferred the definition in Eq. (12) as it leads to a bounded quantity. The threshold θ defines the maximum acceptable distance.

The weighting matrix $\mathbf{W}$ is obtained by maximizing, via Multi-swarm Particles Swarm Optimization (MPSO), the fitness function J. Briefly, in MPSO a multi-initialization with n concurrent swarms is employed [18–20]. Each swarm is moved within a search area to find the optimal solution. After a certain number of optimization epochs, particles are exchanged between swarms to avoid local maxima (see Appendix for details).

2.3. Data simulation

To evaluate the performance of the method, simulated signals were built according to Eq. (1), as described in the following sections.

2.3.1. Atrial activity

Two AA components are considered in the model: background and localized components. The background AA signal was obtained using the autoregressive model

$$a_B(n) = \sum_{k=1}^{p} c_k a_B(n-k) + w(n) \tag{13}$$

where p is the model order and the c_k are the model coefficients. The model parameters (c_k and p) were derived by fitting a set of real AEG signals. Briefly, 10 segments of AEG between two atrial depolarizations, i.e., the background AA, were considered. Each segment was fitted by autoregressive models of order p, with p ranging between 1 and 40. To pool together a common model, once determined the optimal global order by the Akaike information criterion, the corresponding c_k coefficients among the 10 models were averaged.

To simulate the localized AA, the activation of atrial fibers was approximated by a current dipole, $\mathbf{p}$, moving along a straight line.
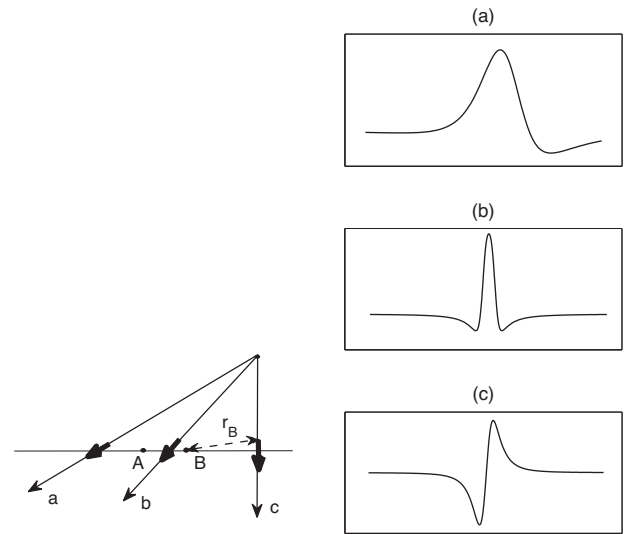

Fig. 2. Left panel: three different directions of the dipole are shown together with the recording site (A and B); r_B exemplifies the distance between the source point of the dipole moving on the c line and the field point B. Right panel: the corresponding atrial potentials $\phi_A - \phi_B$ recorded by the bipolar lead A–B.

The potential generated by this dipole in a uniform infinite medium (with conductivity σ) is [21]

$$\phi = \frac{\mathbf{p} \cdot \mathbf{u}_d}{4\pi \sigma r^2} \tag{14}$$

where $\mathbf{u}_d$ is the unit vector directed from the source point to the field point and r is the distance between these two points. We made the hypothesis that the dipole moves in the medium at constant velocity passing nearby the recording electrodes and that its properties are constant in time (amplitude, direction and versus). Given the fact that we considered bipolar electrograms, the atrial potential is given by $\phi_A - \phi_B$, where A and B are the electrode positions. Fig. 2 shows three different directions of the dipole and the corresponding measured potentials.

2.3.2. Ventricular activity

To build the VA, both the occurrence and the morphology of the wave had to be simulated.

A realistic sequence of RR intervals during AF was generated using the atrioventricular (AV) node model described in Corino et al. [22,23]. The proposed model is defined by parameters that characterize the arrival rate of atrial impulses, the probability of an impulse choosing either one of the two AV nodal pathways, the refractory periods of these pathways, and the prolongation of the refractory periods. The model parameters were chosen to generate RR series with different mean heart rate (HR) (90, 120 and 150 bpm). In particular, the mean arrival rate of AF impulses was varied in the range 5–8 Hz, the refractory period of the slow and fast pathways in the range 0.1–0.4 s and 0.2–0.7 s respectively, with a maximal prolongation of 0.2 s, and the probability of an impulse choosing either one of the two paths ranging between 0.2 and 1.

The ventricular morphology is analogously obtained as the potential generated by a current dipole. Local variations in VA amplitude and width are inserted on a beat-to-beat basis.

2.3.3. Composition of the synthetic AEG

To mimic different degrees of atrial organization according to the three Wells' types, synthetic signals were built. The standard deviation of a_B was varied in the range 0.05–0.2 a.u. a higher variance being associated to higher Wells' type. The position of a_L was selected assuming that atrial depolarizations' front arrives to the electrodes according to a gamma distribution $a_L \sim \Gamma(k, \theta)$, whose
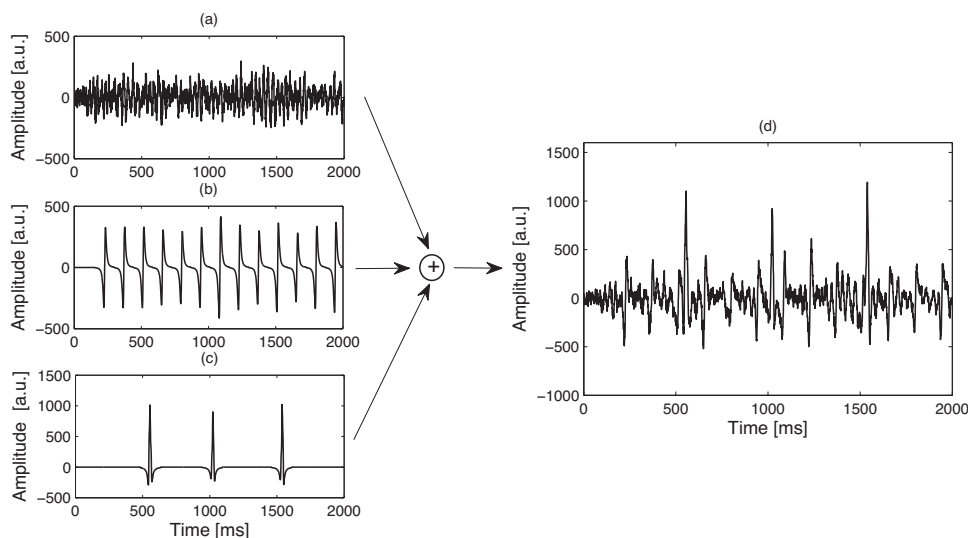
Fig. 3. An example of simulated signal of Wells' type-II with HR of 120 bpm (d) given as the sum of (a) background AA, (b) localized AA and (c) VA (see text for more details).

probability density function is close to an exponential (for small values of k) or to a normal (for high values of k) distribution. Thus, Wells' type-I was simulated using $k = 20$ and $\theta = 10$, Wells' type-II $k = 10$ and $\theta = 14$, and Wells' type-III $k = 1$ and $\theta = 111$, corresponding to an AF rate of 5, 7, and 9 Hz. To have a certain variability in the shape of a_L waves, their morphology was randomly chosen among a set of possible shapes for atrial potentials, obtained using different directions of the dipole (parallel, perpendicular and at 45° in respect to the electrodes line). Finally, the mean amplitude of the VA was defined as two times the mean amplitude of a_L. For each combination of Wells' type and HR, 40 one-minute signals were simulated. An example of type-II with HR of 120 bpm is shown in Fig. 3(d).

2.4. Real data

The proposed algorithm was also tested on electrocardiographic recordings collected in the electrophysiology laboratory of San Paolo Hospital at the University of Milan, from patients undergoing radiofrequency ablation of the pulmonary veins for treatment of AF. The signals were stored in the memory of the Bard recording system during a standardized electrophysiological procedure, exported and anonymized for subsequent analysis. Bipolar electrograms were recorded for 2 min. Eleven recordings obtained from 3 patients in different phases of the electrophysiological study were studied. This investigation was designed as an observational study and it conforms to the principles outlined in the Declaration of Helsinki; the Research Ethics Board of the San Paolo Hospital of the University of Milan, Italy approved the study protocol. All patients were informed about the procedure and gave their written consent.

2.5. Performance evaluation

To quantitatively compare the performances of the algorithms, three indexes were employed.

The first one measures the degree of similarity between the AEG and the residue by means of the normalized mean squared error, defined for each beat as

$$\text{NMSE}^j = \frac{P^j_{s-r}}{P_s} \qquad (15)$$

where j indicates the jth beat, thus P^j_{s-r} is the mean square error between the signal and the residue in a 100 ms window centered in the VA, and P_s is the power of the whole signal s (P are defined as in Eq. (7)). Obviously, the actual AA being unknown in real data, this index can be used to evaluate the cancellation performance on simulated data only.

The second one evaluates the beat-by-beat amplitude reduction of the peak of VA and is defined as

$$\text{VDR} = 10\log_{10}\left(\left|\frac{R^j_s}{R^j_r}\right|\right) \qquad (16)$$

where j indicates the jth beat, R^j_s is the jth peak amplitude of the original AEG in a 100 ms window centered in the VA, and R^j_r is the jth peak amplitude of the residue (i.e., the amplitude of the residue signal at the same position of the peak on the original AEG). High positive values of VDR will indicate good performance of the algorithm. Values close to zero are associated with poor performance and negative values indicate reduction errors because the peak is larger than before. This index was introduced in [13] and therefore computed here for comparison. However, its value is limited. In fact, it must be noted that if the segment containing VA is set to a value close to zero, the VDR would be very high and thus the performance considered optimal. Luckily, in our approach, J_3 avoids this extreme possibility. This index can be computed on simulated data as well as on real recordings.

The third index (PP) evaluates whether the power of the residue is inside the standard range of the atrial power range (AP_{95}), evaluated non-parametrically, i.e., it is within the 2.5 and 97.5 percentiles of the distribution of the values of AA measured on the same data and PP is computed as the percentage of segments whose residual power is outside the standard range AP_{95}. First, the segments containing AA only are divided into 100-ms segments (a new signal segment is defined every ms, and thus, segments overlap), the mean power for each segment computed and the standard range AP_{95} for the specific signal obtained. Then, the power of the residue is computed on the segments containing VA and the percentage of segments whose power was beyond standard range AP_{95} was computed. It should be noted that this index can be used for real data too. Obviously, the quality of the estimates for the residual power will be limited by the length of the ECGs at disposal.
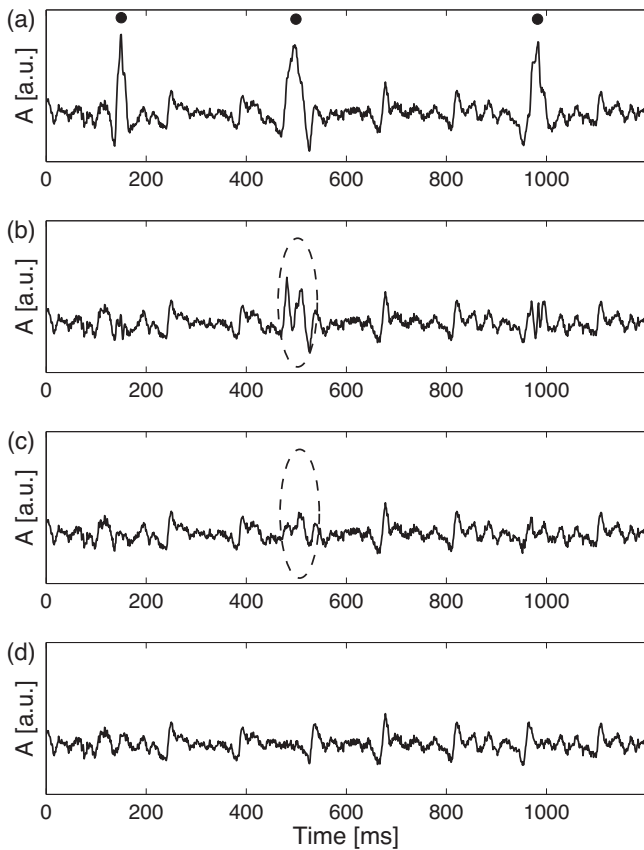
Fig. 4. Example of cancellation of VA from a simulated AEG. (a) Original AEG, where occurrences of VA are identified by black dots. Cancellation obtained by (b) TMS or (c) mTMS. (d) Original atrial signal. A = amplitude.
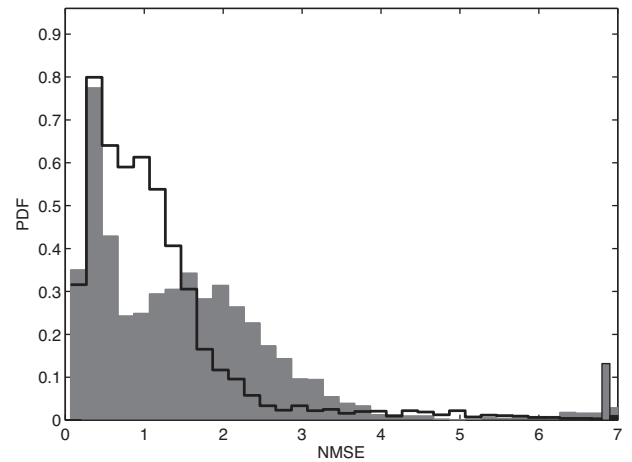

Fig. 5. Histogram of NMSE obtained after removal of VA from simulated signals, using TMS (grey area) or mTMS (black thick line). The signals were Wells' type-III and heart rate of 120 bpm. PDF = probability density function.

2.6. Statistical analysis

The three indexes assessing the performances of the algorithms were computed for TMS and mTMS and compared using the Wilcoxon test. The null hypothesis was that the mean of VDR was higher for TMS than for mTMS, that the mean of NMSE and of PP was lower for TMS than for mTMS. A *p*-value <0.05 was considered statistically significant.

3. Results

The fitness function J depends on the parameters α, β, δ and θ which appear in Eqs. (5) and (11). They were set to the values of:
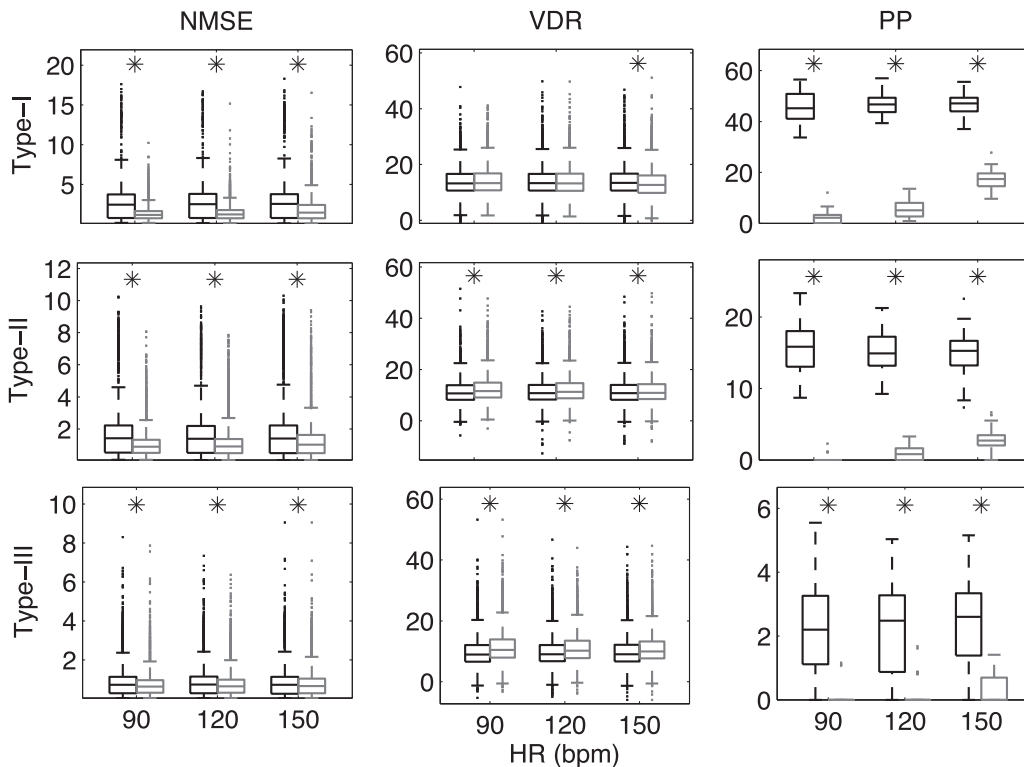

Fig. 6. Boxplots of the indexes assessing performance using TMS (black) and mTMS (grey). Each row shows results for a different Wells' type, whereas each column shows a different index. Each subplot presents results with increasing HR. It can be noted that NMSE and PP are significantly lower for mTMS and VDR higher. $^\ddagger p < 0.05$, $^\dagger p < 0.01$, $^* p < 0.001$.
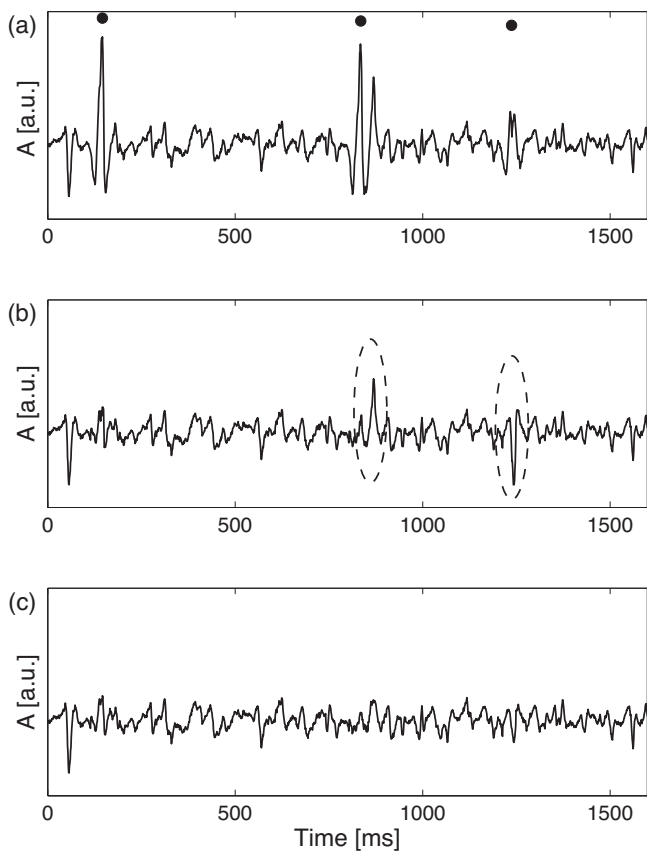
Fig. 7. Example of VA cancellation of a real endocardial signal recorded in the coronary sinus: (a) original AEG with QRS position (black dots) from the surface ECG, residue obtained after (b) TMS and (c) mTMS cancellation. See text for details.

$\alpha = 7$, $\beta = \delta = 1$, and $\theta = 0.4$ with the highest weight to J_1, the power of the residues, meaning that α is the most relevant factor in J. The design of the weight values was aided by simulations which furnished a rough approximation of the relative importance of each term in the problem at hand. A more accurate description of the procedure is given in the Appendix.

3.1. Simulated data

Fig. 4 shows the cancellation of VA from a simulated AEG. A clear residual of VA cancellation is still present when TMS is employed (see ellipses in Fig. 4(b)). Conversely, using mTMS (Fig. 4(c)), a lower remainder of VA is observed.

Fig. 5 shows the histogram of NMSE values obtained on simulated signals from Wells' type-III and HR of 150 bpm. The values of NMSE obtained with mTMS are generally smaller (the histogram is left-shifted in Fig. 5) and, on average, lower errors are obtained.

These results are confirmed on all the sets. Fig. 6 shows the results for the Wells' types and HR. In particular, the values of NMSE are always significantly lower, when using mTMS implying that the residual signals are closer to the original ones, leading to more reliable results. The VDR is higher using mTMS, implying a better cancellation. The PP, i.e., the percentage of segments whose residual power is outside the standard range of atrial power AP_{95} is always lower for mTMS, implying that there are few high-power residual segments.

3.2. Real data

Fig. 7 shows an example of ventricular cancellation on real signals, recorded from the coronary sinus. It can be noted that a

Table 1
Median (25–75% percentiles) of VDR and PP computed on real AEGs.

	TMS	mTMS
VDR		
CS1	6.71 (3.24–9.88)	8.15 (4.91–11.52)[*]
CS2	5.48 (2.01–9.56)	6.82 (3.42–10.84)[*]
CS3	1.44 (0.13–6.08)	2.73 (0.29–7.52)[*]
CS4	0.77 (−0.90 to 3.65)	1.60 (−0.45 to 5.36)[*]
CS5	2.34 (0.51–4.88)	3.39 (1.02–6.34)[*]
PP		
CS1	2.44 (0.38–3.55)	0.38 (0.00–0.97)[*]
CS2	1.65 (1.17–2.72)	0.46 (0.00–0.78)[*]
CS3	1.95 (1.15–3.55)	0.46 (0.00–0.78)[*]
CS4	2.20 (1.43–2.96)	0.48 (0.00–0.99)[*]
CS5	2.54 (1.56–2.86)	0.80 (0–1.18)[*]

[‡] $p < 0.05$.
[†] $p < 0.01$.
[*] $p < 0.001$.

high residual is still present when TMS is employed (see ellipses in Fig. 7(b)); conversely, using mTMS, a lower remainder of VA is observed. The three VA being different from each other (see Fig. 7(a)), the TMS algorithm fails to completely cancel them, as the actual template is highly dependent on the previous one. On the contrary, the higher flexibility in building the template in the mTMS algorithm provides a better cancellation in situations like this.

Comparison of VDR computed for TMS and mTMS is shown in Table 1. In all recording sites (CS1–CS5), VDR is significantly higher for the mTMS algorithm. In addition, moving away from the ventricles (from CS1 to CS5) VDR decreases, probably because of the larger distance from the ventricles which implicitly reduces the amplitude of the ventricular complexes and their relevance on the AA. In fact, the amplitude of the VA on the original AEGs (normalized to the background noise) decreases moving from CS1 to CS5, from 3 ± 1 in CS1 to 1.8 ± 0.5 in CS5.

Table 1 also shows the atrial power values for TMS and mTMS. A statistically significant reduction in PP can be noted in all recording sites, in particular in CS1 which is the closest to the ventricles. Value for the NMSE cannot be computed on real data, the true AA being unknown.

4. Discussion

Cancellation of VA in AEG is the most important preliminary step for almost all further analyses of AEG. Beat-to-beat variability in the morphology of the QRS complex might induce the TMS method to leave ahead residuals of cancellation with large localized power. To overcome this problem, while constraining the shape of the template not to vary too much from what is suggested by TMS, we modulated its shape, via an optimization procedure, so that the power of each AEG interval after cancellation is constrained to have power levels similar to the nearby atrial activity.

The main findings of this study are: (i) the modulation of the TMS template improves the cancellation of VA from AEG during AF; (ii) the performance of the proposed method is largely independent (at least in the range tested) of ventricular rate or AEG organization.

We showed using both synthetic signals and AEGs recorded during routine ablation procedures that the proposed approach is superior to TMS alone. When compared with the results of a previous study addressing the same issue [13], we note that: (i) VDR was on average comparable to the values previously reported; (ii) mTMS did not alter AEG signal outside the ventricular segment at variance of methods based on independent components and of TMS when large averaging windows are employed as in [13]; (iii) mTMS was firstly tested on simulated data which permitted a limited but objective performance evaluation.

This work expands the concept we have recently proposed in [16]: i.e., to modulate the TMS template to obtain better VA cancellation. While in [16] a preliminary attempt to solve the problem of TMS poor cancellation has been anticipated, this work formalizes the solution. In particular, we showed that the new proposed strategy (i.e., to modulate the template to keep the residual power in the range of the expected atrial one) provides very good results and we quantified the improvement in respect to TMS alone. Such improvements were observed not only on simulated data but also on patient recordings and were documented by several metrics employed to evaluate cancellation performances. A limitation of the study is that the method was tested on signals collected only from three different patients. While the extensive analysis made on synthetic signals offered a severe methodological workbench, tests on larger dataset are surely necessary for a thorough clinical evaluation. Also, due to the small number of patients, no side effect was evaluated.

A limit of our approach is that temporal relations among samples are lost. In fact, the elements of the diagonal matrix **W** are selected independently from each other by MPSO. The problem might become relevant when the residual signal contains localized atrial activity. In fact, in these situations, part of such activity might be inadvertently canceled along with the ventricular one. However, the results of our simulations showed that, with the parameters selected in the fitness function, this problem is of limited importance.

Finally, in this work we employed MPSO for the selection of the coefficients. Other algorithms could have been used, however the large number of members that compose the particle swarm makes MPSO impressively resilient to the problem of local maxima, in comparison to other global maximization strategies such as simulated annealing [24]. Unfortunately, the computational requirements of MPSO are significant and mTMS has a larger computational time than TMS alone.

Competing interests

None declared.

Funding

None.

Ethical approval

This investigation was designed as an observational study and it conforms to the principles outlined in the Declaration of Helsinki; the Research Ethics Board of the San Paolo Hospital of the University of Milan, Italy approved the study protocol. All patients signed a written informed consent.

Appendix A. Particle Swarm Optimization

Particle Swarm Optimization (PSO) is an iterative computational method able to solve optimization problems [18]. The idea behind the algorithm is simple: a swarm of M particles (representing the problem's solution) is moved within a search area to find the optimal spot (the solution to a given problem). At each iteration step, M potential solutions are obtained and, among them, the best one is selected (i.e., the one which maximizes a predefined, problem-specific *fitness function*). These intermediate solutions are used for the movement of particles in successive iteration, i.e., the particles are pushed to move towards them. The process is repeated until a stop criterion is reached.

The algorithm employed in this work is an extension of PSO termed Multi-swarm Particle Swarm Optimization (MPSO) [17]. In MPSO a multi-initialization with n concurrent swarms is employed. The search space is enlarged by exchanging particles between swarms after a fixed number of iterations (the worst solution is traded for the best one of another swarm). The algorithm is robust with respect to local optimal solutions because it is not based on the gradient of the function to maximize.

The topology of the set of swarms, the number of particle exchanged across them and the number of iterations before swaps of particles play a fundamental role for the convergence time. If the exchange is done too early, the convergence time increases. However, if done after too many iterations, the risk of falling into local maxima increases. In this work, we tried to balance between these two issues. We selected a ring topology with 10 swarms of 12 particles each. Swarms were initialized into a hypersphere of center equal to 1. Every 10 iterations, 5 particles were exchanged from a swarm to another. The stopping criterion was either reaching the maximum number of iterations (1000) or reaching 99.9% of the maximum value of the fitness function, i.e., $\alpha + \beta$, see Eq. (5). Regarding the selection of the fitness function employed in this work, it was built in Eq. (5) as a linear combination of sub-functions $J(x) = \sum_{i=1}^{N} \lambda_i J_i(x)$ to solve a multi-goal optimization problem. To avoid having one $J_i(x)$ predominant over the others, we built each of them as in Eq. (6) with a progressive derivative that penalizes solutions distant from the optimum. In this way the swarms compete and cooperate to reach the optimal solution once the values of λ_i are balanced and coherent with the objective of the optimization.

The values of λ_i could be given empirically. In this work we preferred to study their influence on the final result before taking a choice. Several values of the parameters α, δ and θ (β was set to 1 in advance with no lack of generality) were tested with the mTMS method on two sets of simulated signals with 60 ventricular activities each. They were generated as in Section 2.3.3 with different organization and HR. For each set of parameters we computed the metric

$$I(\alpha, \delta, \theta) = (C - 1)^2 + \text{NMSE}^2, \tag{A.1}$$

which takes into account both the normalized mean square error and the linear correlation C. A large value of C means that the shape of the modulated template is preserved in mTMS, whereas a small value of NMSE forces a larger departure from the TMS template. Both these issues must be taken into account as described in the main text.

To further guide our selection, we also employed a second MPSO algorithm to minimize the metric I, but this time having as variables the parameters α, δ and θ. Their final value jointly minimizes the NMSE and maximizes the linear correlation C. The results obtained were $\alpha = 6.97$, $\delta = 0.99$ and $\theta = 0.43$ which prompted our final choice: $\alpha = 7$, $\delta = 1$ and $\theta = 0.4$. A typical computation of the matrix W on an Intel Xeon E5-1620 (Quad Core, 3.60 GHz) took 3.5 s.

References

[1] Wells J, Karp RB, Kouchoukos NT, MacLean WA, James TN, Waldo AL. Characterization of atrial fibrillation in man: studies following open heart surgery. Pacing and Clinical Electrophysiology 1978;1:426–38.

[2] Forclaz A, Narayan SM, Scherr D, Linton N, Jadidi AS, Nault I, et al. Early temporal and spatial regularization of persistent atrial fibrillation predicts termination and arrhythmia-free outcome. Heart Rhythm 2011;8:1374–82.

[3] Ravelli F, Faes L, Corino V, Mainardi L. Organization measures of atrial activity during fibrillation. In: Sornmo L, Cerutti S, Mainardi L, editors. Understanding atrial fibrillation: the signal processing contribution. San Francisco: Morgan-Claypool; 2008. p. 127–50.

[4] Mainardi L, Porta A, Calcagnini G, Bartolini P, Michelucci A, Cerutti S. Linear and non-linear analysis of atrial signals and local activation period series during atrial-fibrillation episodes. Medical & Biological Engineering & Computing 2001;39:249–54.

[5] Everett TH, Kok LC, Vaughn RH, Moorman JR, Haines DE. Frequency domain algorithm for quantifying atrial fibrillation organization to increase defibrillation efficacy. IEEE Transaction on Biomedical Engineering 2001;48(9):969–78.

[6] Mainardi L, Corino VDA, Lombardi L, Tondo C, Mantica M, Lombardi F, et al. Assessment of the dynamics of atrial signals and local atrial period series during atrial fibrillation: effects of isoproterenol administration. Biomedical Engineering 2004;3:37 [Online].

[7] Ropella KM, Sahakian AV, Baerman JM, Swiryn S. The coherence spectrum, a quantitative discriminator of fibrillatory and nonfibrillatory cardiac rhythms. Circulation 1989;80:112–9.

[8] Mainardi L, Corino V, Lombardi L, Tondo C, Mantica M, Lombardi F, et al. Linear and nonlinear coupling between atrial signals, three methods for the analysis of the relationships among atrial electrical activities in different sites. IEEE Engineering in Medicine and Biology Magazine 2006;25:63–70.

[9] Censi F, Barbaro V, Bartolini P, Calcagnini G, Michelucci A, Gensini GF, et al. Recurrent patterns of atrial depolarization during atrial fibrillation assessed by recurrence plot quantification. Annals of Biomedical Engineering 2000;28:61–70.

[10] Faes L, Nollo G, Kirchner M, Olivetti E, Gaita F, Riccardi R, et al. Principal component analysis and cluster analysis for measuring the local organisation of human atrial fibrillation. Medical & Biological Engineering & Computing 2001;39:656–63.

[11] Faes L, Nollo G, Antolini R, Gaita F, Ravelli F. A method for quantifying atrial fibrillation organization based on wave-morphology similarity. IEEE Transaction on Biomedical Engineering 2002;49:1504–13.

[12] Sih HJ, Zipes DP, Berbari EJ, Olgin JE. A high-temporal resolution algorithm for quantifying organization during atrial fibrillation. IEEE Transaction on Biomedical Engineering 1999;46:440–50.

[13] Rieta JJ, Hornero F. Comparative study of methods for ventricular activity cancellation in atrial electrograms of atrial fibrillation. Physiological Measurement 2007;28:925–36.

[14] Alcaraz J, Rieta JJ. Adaptive singular value cancelation of ventricular activity in single-lead atrial fibrillation electrocardiograms. Physiological Measurement 2008;29:1351–69.

[15] Bollmann A, Husser D, Mainardi L, Lombardi F, Langley P, Murray A, et al. Analysis of surface electrocardiograms in atrial fibrillation: techniques, research, and clinical applications. Europace 2006;8:911–26.

[16] Mainardi L, Rivolta M, Scanziani R, Corino V, Sassi R. Cancellation of ventricular activity in endocavitary recordings during atrial fibrillation by particle swarm optimization. In: Proceedings of computing in cardiology. 2011. p. 597–600.

[17] Vanneschi L, Codecasa D, Mauri G. A study of parallel and distributed particle swarm optimization methods. In: Proceedings of the 2nd workshop on Bio-inspired algorithms for distributed systems (BADS'10). New York, NY, USA: ACM; 2010. p. 9–16.

[18] Kennedy J, Eberhart R. Particle swarm optimization. In: Proceedings of IEEE international conference on neural networks, IV. 1995. p. 1942–8.

[19] Van den Bergh F, Engelbrecht AP. A cooperative approach to particle swarm optimization. IEEE Transactions on Evolutionary Computation 2004;8: 225–39.

[20] Niu B, Zhu Y, He X, Wu H. MCPSO: a multi-swarm cooperative particle swarm optimizer. Applied Mathematics and Computation 2007;2:1050–62.

[21] Malmivuo J, Plonsey R. Bioelectromagnetism: principles and applications of bioelectric and biomagnetic fields. New York: Oxford University Press; 1995.

[22] Corino V, Sandberg F, Mainardi L, Sörnmo L. An atrioventricular node model for analysis of the ventricular response during atrial fibrillation. IEEE Transaction on Biomedical Engineering 2011;58:3386–95.

[23] Corino VDA, Sandberg F, Lombardi F, Mainardi LT, Sörnmo L. Atrioventricular nodal function during atrial fibrillation: model building and robust estimation. Biomedical Signal Processing and Control 2013, http://dx.doi.org/10.1016/j.bspc.2012.10.006.

[24] Vanneschi L, Codecasa D, Mauri G. A comparative study of four parallel and distributed PSO methods. New Generation Computing 2011;29:129–61.